NASA TECHNICAL NOTE

NASA TN D-2435

NASA TN D-2435

LAMINAR AND TURBULENT HYDROGEN HEAT TRANSFER AND FRICTION COEFFICIENTS OVER PARALLEL PLATES AT 5000° R

by Jack G. Slaby, William L. Maag, and Byron L. Siegel

Lewis Research Center
Cleveland, Ohio

NATIONAL AERONAUTICS AND SPACE ADMINISTRATION • WASHINGTON, D. C. • AUGUST 1964

LAMINAR AND TURBULENT HYDROGEN HEAT TRANSFER AND FRICTION COEFFICIENTS OVER PARALLEL PLATES AT 5000° R

By Jack G. Slaby, William L. Maag, and Byron L. Siegel

Lewis Research Center
Cleveland, Ohio

NATIONAL AERONAUTICS AND SPACE ADMINISTRATION

For sale by the Office of Technical Services, Department of Commerce,
Washington, D.C. 20230 -- Price $0.75

LAMINAR AND TURBULENT HYDROGEN HEAT TRANSFER AND FRICTION COEFFICIENTS OVER PARALLEL PLATES AT 5000° R

by Jack G. Slaby, William L. Maag, and Byron L. Siegel

Lewis Research Center

SUMMARY

Local heat-transfer coefficients and average friction factors were obtained experimentally for hydrogen flowing over parallel tungsten plates heated electrically to 5000° R with an outlet hydrogen temperature as high as 3500° R. For these experiments, the ratio of length to equivalent diameter was 74, and the modified Reynolds number varied from 1255 to 12,500 with the fluid properties evaluated at the film temperature. The ratio of surface to bulk-gas temperature extended to 3.0, and the maximum local heat flux was 2.75 Btu per second per square inch.

The local heat-transfer coefficients for turbulent flow were correlated by a Dittus-Boelter-type equation. The experimental laminar-flow heat-transfer data showed good agreement with an analytical study of a developing laminar-flow region. The thermal entrance length required for a constant Nusselt number in laminar flow depended on the local modified film Reynolds number, which decreased as much as a factor of 3 from entrance to exit. An experimental value of Nusselt number equal to 9.0 was determined for fully developed laminar flow across parallel plates.

The experimental friction factors in the laminar entrance region of parallel plates agreed with average analytical friction factors in the laminar entrance region of a tube. Average isothermal turbulent friction factors correlated with the Kármán-Nikuradse line. With the addition of heat, however, the friction factors were progressively higher than the Kármán-Nikuradse line.

INTRODUCTION

The primary objective in the design of a solid-core nuclear rocket engine is to achieve the highest hydrogen propellant temperature within the operating

limits of the materials of the core. In this manner a high specific impulse can be obtained to perform the more advanced interplanetary missions. A successful design depends on finding solid materials that can operate at high temperatures under high aerodynamic forces and being able to predict accurately the heat-transfer rates for the hydrogen - solid-core system at these temperatures. Experimental research at the Lewis Research Center is being performed to determine (1) the effect of internal heat generation and high temperatures on the structural properties of tungsten and other refractory materials, (2) the effect of high aerodynamic forces on various fuel element configurations at elevated temperatures, and (3) the effect of variable thermodynamic and transport properties of hydrogen on existing convective heat-transfer and friction-factor correlations.

The operating conditions that would exist in a solid reactor core can be simulated by flowing hydrogen over electrically heated elements. A parallel-flat-plate configuration was chosen for this study because it can be electrically heated. This type of testing, in which nuclear heating is simulated electrically, permits study of heat-transfer and multipassage-flow-distribution problems. Previous experimental heat-transfer data (refs. 1 to 4) at high surface temperatures have been presented for single tubes, but few or no data exist for parallel-plate configurations. This report deals with the heat-transfer aspect of this project and extends the convective-heat-transfer and friction-factor correlations for a hydrogen - parallel-plate system up to surface temperatures of 5000° R.

SYMBOLS

A free-flow cross-sectional area at spacers, sq ft

A_{fr} spacerless free-flow cross-sectional area, sq ft

A_e current-flow cross-sectional area, sq ft

C constant

C_{co} conversion constant, electric to thermal heat, 0.948×10^{-3} Btu/(sec)(w)

c_p specific heat of hydrogen at constant pressure, Btu/(lb)($^{\circ}$R)

D equivalent diameter of test section at spacer cross section, ft

D_{fr} equivalent diameter of test section at spacerless cross section, ft

f average friction factor

G mass velocity at spacerless cross section, lb/(sec)(sq ft)

G_{max} mass velocity at spacer cross section, lb/(sec)(sq ft)

Gr Graetz number, $Re_f Pr_f/(x/D)$

g	acceleration due to gravity, 32.2 ft/sec^2
H	enthalpy, Btu/lb
h	local heat-transfer coefficient, Btu/(sec)(sq ft)($^\circ$R)
I	current, amp
K_c	test-section-entrance contraction coefficient
K_{cs}	spacer contraction coefficient
K_{es}	spacer expansion coefficient
k	thermal conductivity of hydrogen, Btu/(ft)(sec)($^\circ$R)
L	test-section length, ft
N	number of sets of spacers
Nu	Nusselt number, hD/k
ΔP	static pressure drop across test section, lb/sq ft
Pr	Prandtl number, $c_p\mu/k$
p	absolute static pressure, lb/sq ft
q	rate of heat transfer to hydrogen, Btu/sec
Δq	incremental rate of heat transfer, Btu/sec
q_{gen}	rate of electric heat input, Btu/sec
R	resistance, ohms
Re	Reynolds number, $G_{max}D/\mu$
Re_f	modified film Reynolds number, $\frac{G_{max}D}{\mu_f}\frac{T_b}{T_f}$
$\mathfrak{R}_g$	gas constant, ft-lb/(lb)($^\circ$R)
S	total heat-transfer surface area, sq ft
S_{fr}	total friction surface area, sq ft
T	total or stagnation temperature, $^\circ$R
T_b	average bulk temperature, $(T_{in} + T_{out})/2$, $^\circ$R
T_f	average film temperature, $(T_s + T_b)/2$, $^\circ$R

T_s average surface temperature, $^{\circ}R$

t static temperature, $^{\circ}R$

V local bulk velocity of gas, ft/sec

$\mathcal{V}_e$ voltage, v

v local velocity of gas, ft/sec

W gas-flow rate, lb/sec

x distance from entrance of test section, ft

Z spacer pressure factor

α deviation of velocity profile from uniform (slug-flow) velocity profile for which $\alpha = 1$

γ ratio of specific heats of hydrogen

Δ_t thermal boundary-layer thickness

δ hydrodynamic boundary-layer thickness

ζ resistivity of tungsten, (ohm)(ft)

ρ density of gas, lb/cu ft

ρ_m mean density of gas, $(p_{in} + p_{out})/\mathcal{R}_g(t_{in} + t_{out})$, lb/cu ft

σ ratio of spacerless free flow area to frontal area

μ absolute viscosity of hydrogen, lb/(sec)(ft)

τ_w wall shear stress, lb/sq ft

Subscripts:

av average

b bulk (when applied to properties, indicates evaluation at average bulk temperature T_b)

cond conduction

conv convection

e electric

f film (when applied to properties, indicates evaluation at average film temperature T_f)

fr	friction
g	gas
gen	generated
in	entering test-section apparatus
m	mean
mo	momentum
noz	nozzle
out	leaving test-section apparatus
rad	radiation
s	surface (when applied to properties, indicates evaluation at average surface temperature T_s)
x	characteristic length dimension
0,n+1	test-section inlet and outlet, respectively
0,1,2,3,4,5	stations, refer to fig. 3

APPARATUS AND PROCEDURE

Flow System

The flow system is shown schematically in figure 1. Hydrogen, supplied from a bank of high-pressure bottles at ambient temperature, was metered through a choked flow nozzle and controlled with a remotely operated pressure control valve. The use of a choked flow nozzle assured constant mass flow through the test section as long as a choked condition was maintained in the nozzle for a constant upstream density. For the nozzle, minimum flow was about 0.008 pound per second, and maximum flow was 0.05 pound per second. The entire system was purged with nitrogen before the hydrogen was turned on. The controls were set for "fail-safe" operation so that the nitrogen purge would automatically come on and both the hydrogen and the electrical supplies would shut down if a predetermined operating permissive failed. The maximum allowable test-section pressure was 75 pounds per square inch absolute. The heated hydrogen was cooled below 1000° R in a concentric-tube hydrogen-to-water heat exchanger before being exhausted through piping to the atmosphere above the building.

Power Supply

A single-phase, 60-cycle, 500-kilovolt-ampere saturable-reactor controlled

power supply was used to heat the elements. Output voltage was varied from 2.5

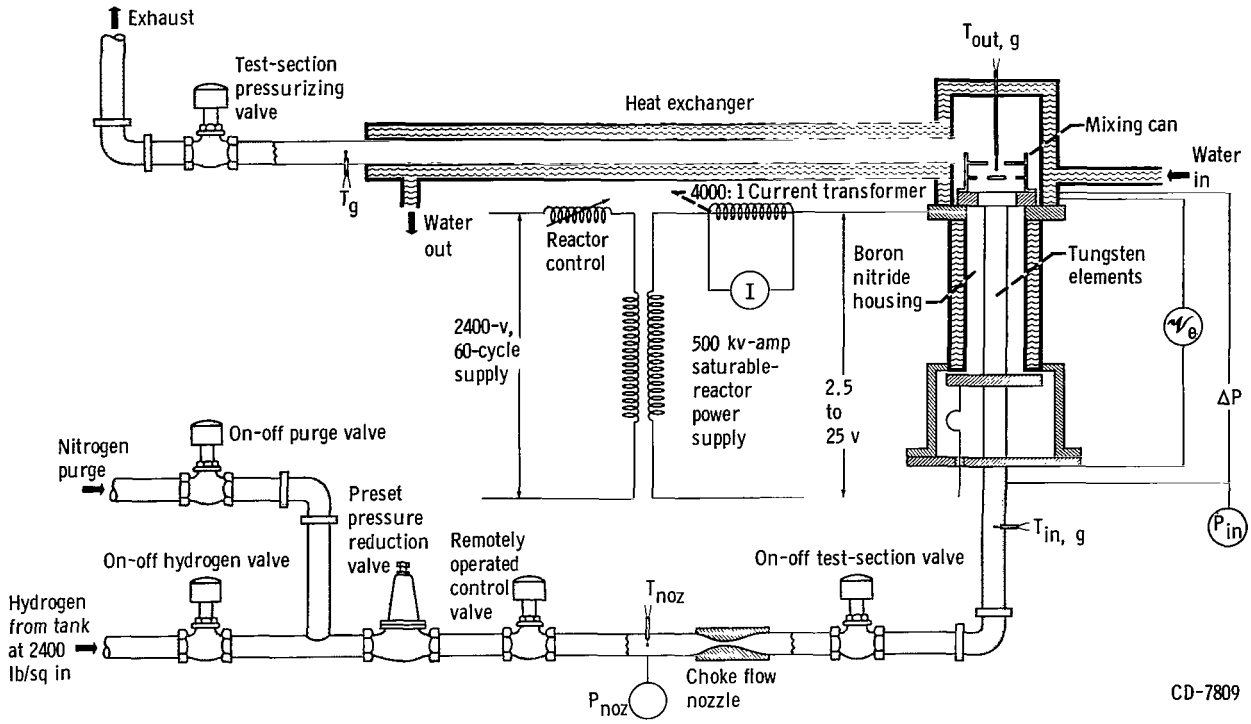

Figure 1. - Schematic diagram of test-section apparatus and location of instrumentation.

to 25 volts with a maximum current rating of 20,000 amperes. With bus losses, however, the maximum power to the test section was limited to 225 kilowatts.

Test Section

Experiments were performed in a test section (figs. 2 and 3) consisting of five commercially rolled tungsten plates, 0.030 inch thick, 1 inch wide, and $9\frac{1}{2}$ inches long, with tabs on each end that served as bus connections. The tabs, which were formed by grinding, connected the elements mechanically and electrically and allowed the hydrogen to flow unimpeded between the plates. The plates were connected in parallel electrically and spaced 0.060 inch apart by tungsten spacers. The spacers consisted of 0.120-inch-outside-diameter tungsten cylinders having a height of 0.060 inch and an inside diameter of 0.065 inch. The spacers were placed over 0.065-inch holes disintegrated in the tungsten plates (3/16 in. from the edge), and a 0.060-inch tungsten bolt was inserted through the five plates and four spacers. A tungsten nut held the assembly together. Two spacer assemblies were located at each 1/2-inch interval along the assembly length, the total being 15 sets (fig. 2). The spacers were necessary to support the plates against the pulsating electromagnetic forces generated by the large alternating current through the plates. Steady-state alternating-current values as high as 14,000 amperes produced loadings on the

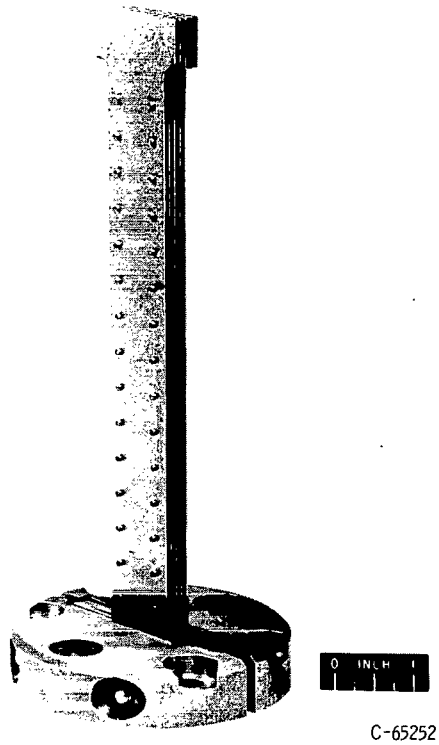

Figure 2. - Five-plate spacer-supported tungsten test section clamped in electrical bus support.

outside plates as high as 3 pounds per inch of length (ref. 5). At the start of a test, transient currents over 100,000 amperes, as measured on an oscilloscope, produced electromagnetic forces large enough to shatter unsupported tungsten plates. Alternating current flowing in the same direction in parallel plates causes the outer plates to pull in toward the center plate and then recover as the current varies from zero to a maximum. The calculated natural frequency of vibration of an unheated tungsten plate, as described previously, supported only at the ends is about 80 cycles per second (ref. 6). The driving frequency of a 60-cycle-per-second alternating-current power supply is 120 cycles per second. High-speed movies taken of a test section with and without supporting spacers showed that, under the influence of a large alternating current, the unsupported test section vibrated like a set of rubber bands. This vibration was probably due to resonance.

The tungsten spacers and pins also supported the plates against aerodynamic forces that cause the plates to vibrate and shatter. A single 9.5-inch-long unsupported plate with no current flow and hence no electromagnetic forces has vibrated itself to pieces under hydrogen flow with a dynamic head as low as 0.1 pound per square inch.

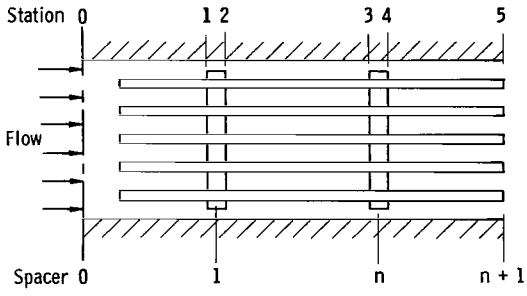

Figure 3. - Schematic of plates and spacers.

The test section (fig. 4) was surrounded by a high-temperature electrical insulator (boron nitride) housing having a flow passage 1/2 by 1 inch in cross section to restrict the hydrogen coolant flow over and between the plates. The boron nitride housing consisted of two inner halves (≈1.5-in. O.D.) held together by a cylindrical 3-inch-outside-diameter outer housing.

In order to take care of longitudinal expansion of the five elements as a unit, a predetermined spring force was applied to one end of the vertically supported elements, while the other end was rigidly fastened. At maximum operating temperature, a slight tension still existed so that the elements would not buckle and cause maldistribution of flow. This arrangement can be seen in figure 4. The inlet bus to the test section was connected by the water-cooled electrodes, which also acted as springs to maintain tension in the test section.

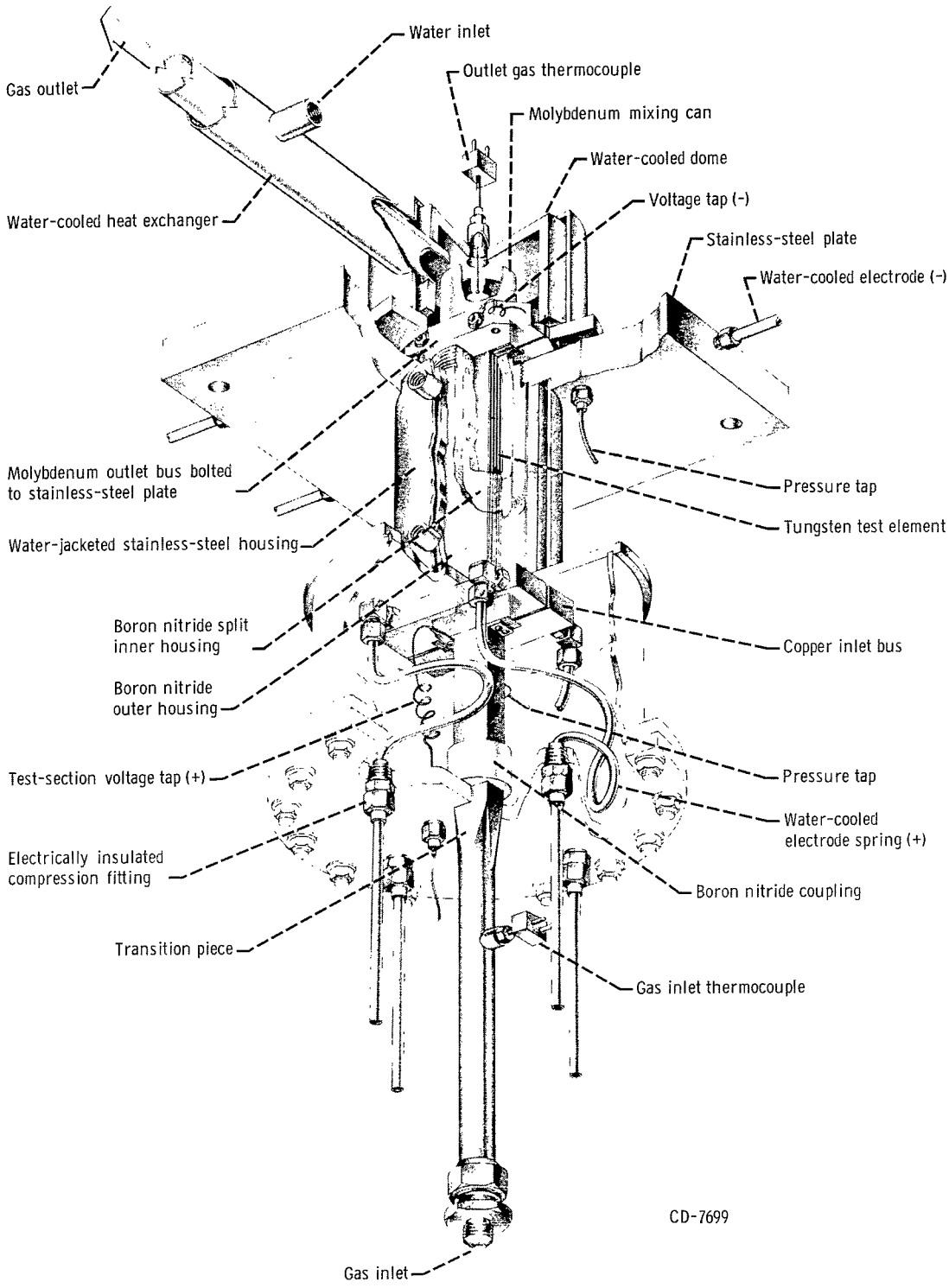

Figure 4. - Cutaway drawing of test section and associated apparatus.

Instrumentation

A schematic of the instrumentation is shown in figure 1. The voltage across and the current through the test section were measured. The test voltage had to be taken directly across the test section because the large current caused appreciable voltage drop in the water-cooled buses between the power supply and the test section. A true-root-mean-square voltmeter was used to measure the test voltage because of the waveform produced by the saturable-reactor controlled power supply. Current was recorded on a recording ammeter and also read on a precision ammeter through a 4000:1 stepdown current transformer. Inlet pressure to the test section was measured with a calibrated 0- to 100-pound-per-square-inch Bourdon tube gage. The pressure drop across the test section was continuously recorded with a temperature-compensated strain-gage bridge pressure transducer. Inlet temperature was measured with a type K thermocouple (designation from ref. 7), and the exit temperature was measured with either a platinum - platinum-13-percent-rhodium or a tungsten - tungsten-26-percent-rhenium thermocouple. The exit thermocouple was placed in a baffled molybdenum mixing can so that it would record a true mixed or bulk gas temperature. The reliability of this measured exit hydrogen temperature was verified by a heat balance on the hydrogen-water heat exchanger located at the test-section exit. Pressure and temperature measurements at the inlet to the choked flow nozzle were made. The mass-flow rate was set by adjusting the nozzle inlet pressure. Test flow rates ranged from 0.0082 to 0.023 pound per second. Measurement of the wall temperature was somewhat difficult because of the high temperatures involved and the complexity of the multipassage test section. It was determined that reliable wall temperatures could be measured by imbedding tungsten - tungsten-26-percent-rhenium thermocouples in the edge of the center plate to minimize radiation errors. Two 0.010-inch-diameter holes, 1/8 inch deep and 0.030 inch between centers, were disintegrated into the edge of a 0.030-inch-thick tungsten element. During the disintegration process, the 1/8-inch-deep holes became slightly tapered. The 0.010-inch-diameter tungsten - tungsten-26-percent-rhenium-thermocouple wire was mechanically wedged into the tapered holes and was found to reliably measure the plate temperature.

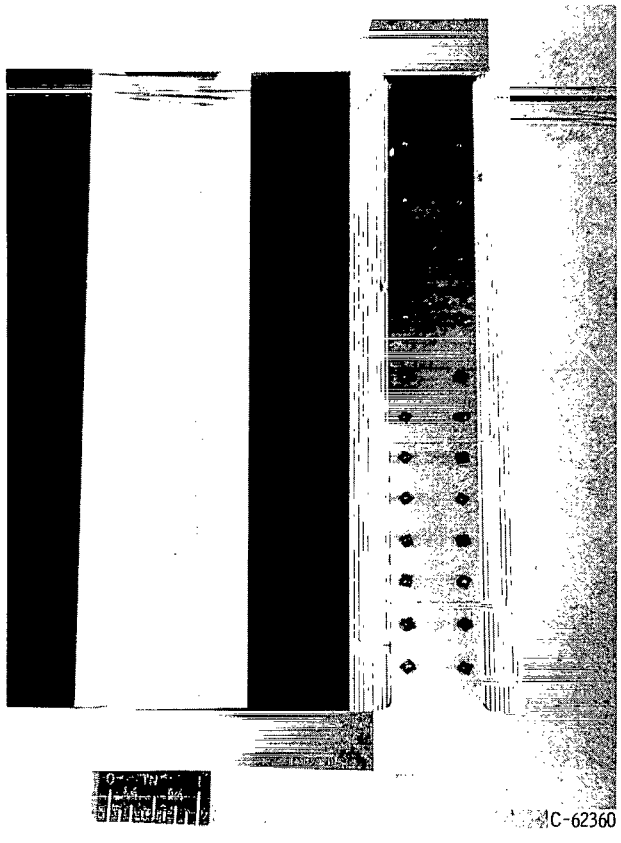

Figure 5. - Tungsten-plate test section instrumented with thermocouples and housed in split boron nitride.

Figure 5 illustrates an instrumented test section. Five tungsten plates stacked one on top of the other were held together by tungsten pins, spacers, and nuts. The eight thermocouples imbedded in the center plate were concentrated near the exit end of the test section (bottom of the picture) because the temperature gradients were larger at the hot end. The gaps left in the boron nitride allowed the tungsten plates to move relative to the boron nitride housing without shearing off the thermocouples. Verified wall temperature profiles are described in the section METHOD OF CALCULATION.

This mechanical joint thermocouple proved to give reliable temperature readings, was easy to install, and did not obstruct the flow passage. It should be cautioned that, once the thermocouple wires were cycled above their recrystallization temperature, they became brittle and subject to breakage. This type of thermocouple is difficult to use with direct-current power because the junction is not a point contact, and, therefore, the thermocouple electromotive force is altered by the distance between the two wires.

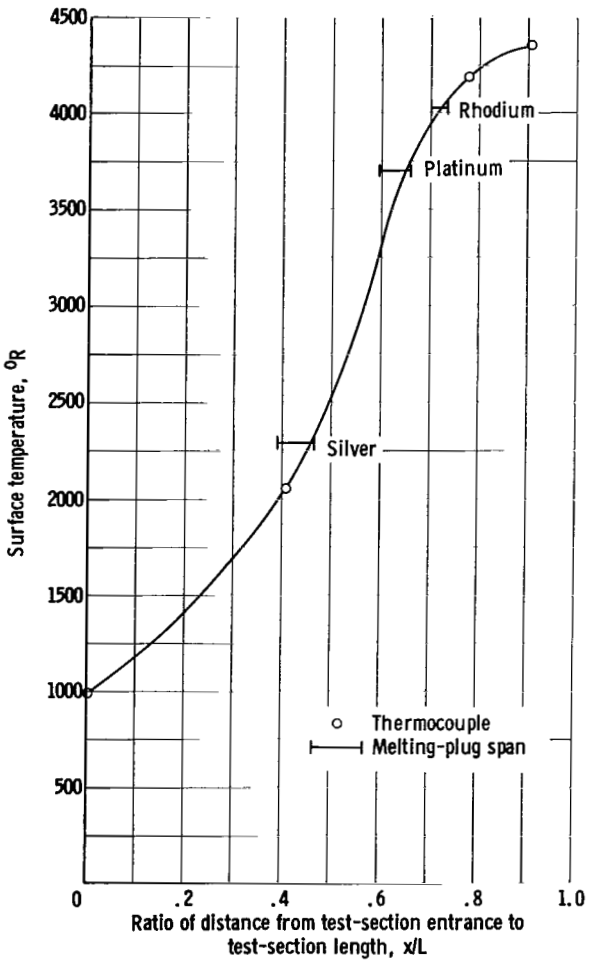

Figure 6. - Typical surface temperature profile of electrically heated five-plate experiment obtained from thermocouple and melting-plug data.

The reliability of the thermocouple readings was initially verified by using melting plugs of noble metals. Small holes of 0.015-inch diameter were disintegrated through the tungsten plates. A series of three to five melting plugs of either silver (m.p., 2200° R), platinum (m.p., 3683° R), or rhodium (m.p., 4031° R), was placed in these holes at intervals about 1/4 inch apart, where the temperature would be near the melting point for each metal. The plugs were actually made like small rivets, peened over on each side, and filed off so that all surfaces were flush. The plates were run at the same power level and gas flow rate as in a previous run in which thermocouples had been used. The wall temperature profiles for each run are similar, as shown in figure 6. The melting plugs also verified that all plates operated at the same temperature. Plugs placed on all five plates melted at the same axial position.

Properties

The physical properties of hydrogen used for all calculations were taken from reference 8.

METHOD OF CALCULATION

Heat Transfer

Local heat-transfer coefficients are calculated because local heat flux and wall temperature profiles vary axially as much as a factor of 5. The test section is divided into 10 equal increments. Both a test element and a wall temperature profile are shown schematically in figure 7. A voltage measurement across the test section is taken for the interval between $x/L = 0$ and $x/L = 1.0$, which corresponds to line FD on the wall temperature profile. This represents the length of the test section in which electrical current generates a measurable amount of heat. Although some heat is generated in the tab portion of the element upstream of $x/L = 0$, the amount is not significant because of the low resistance of the cooled tungsten and copper busing.

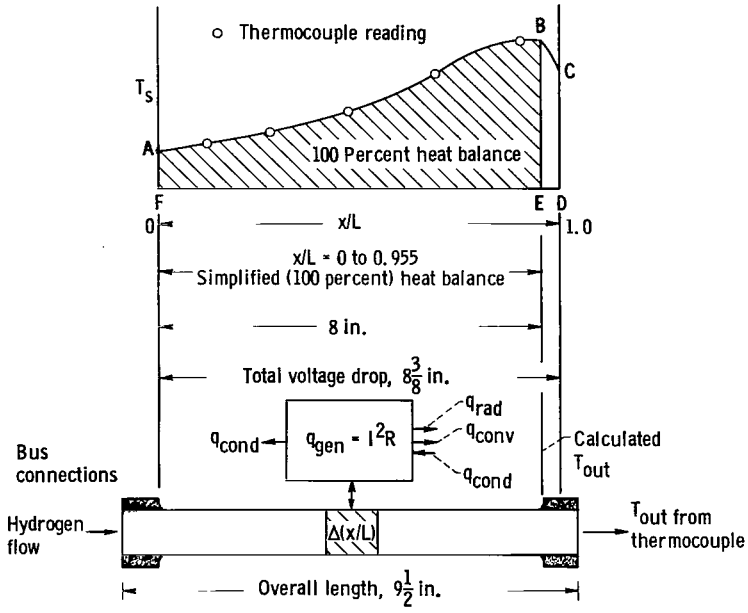

Figure 7. - Model for calculations.

The following simplifying assumptions relating to the incremental element $\Delta(x/L)$ of the 8-inch test section in figure 7 were made:

(1) Axial conduction is negligible ($q_{cond,in} \approx q_{cond,out}$). For the most extreme temperature profiles, the difference between the heat conducted into an increment and the heat conducted out of the increment is less than 1 percent of the total internal heat generated per increment.

(2) Radiation loss is negligible ($q_{rad} \approx 0$). The five tungsten plates radiate to the boron nitride housing from essentially only two of the 10 surfaces. In addition, boron nitride has a highly reflective surface. The radiation heat loss per increment is calculated to be less than 1 percent of the internal heat generated per increment.

(3) In the 10th increment, heat is conducted into the buses and water-

cooled plates and causes a drop in the wall temperature (line BC in fig. 7). The hot hydrogen is also cooled by passing over the colder surfaces in this region. It is almost impossible to take a heat balance on this bus-connected increment. Consequently, the 10th increment is shortened to extend only to $x/L = 0.955$ (point B in fig. 7).

When these assumptions are used, the internal heat generated in the plates (I^2R) equals the amount of heat convected into the hydrogen gas stream for each increment from $x/L = 0$ to $x/L = 0.955$:

$$q_{gen} = \frac{C_{co} I^2 \zeta \, \Delta L}{A_e} = W(H_{out} - H_{in})$$

About 95 percent of the total input power is generated in the region $x/L = 0$ to $x/L = 0.955$. Local heat-transfer coefficients in this region are calculated. The incremental heat-transfer coefficient is then calculated by

$$h = \frac{\Delta q}{\Delta S(T_s - T_b)}$$

where h is an average local coefficient for the increment, which includes 10 surfaces for the five plates, $T_b = (T_{out} + T_{in})/2$, and ΔS is the incremental heat-transfer area of the five plates and spacers. The Nusselt number is calculated by using the relation $Nu = hD/k$. All hydrogen properties are evaluated at the total film temperature, which is essentially equal to the static film temperature at the low Mach numbers of this investigation.

After the hydrogen-flow rate is adjusted and the power level is set, a voltage measurement is taken across the test section between $x/L = 0$ and $x/L = 1.0$. The voltage divided by the current through the test section yields the overall resistance of the test section. When the ratio L/A_e of the plates is known, a value of average resistivity is calculated. The overall average surface temperature is obtained from the relation that exists between temperature and resistivity for tungsten. This average surface temperature is compared with the average surface temperature obtained by integrating the wall temperature profile measured with thermocouples. The two independent methods of measuring the average wall temperature profiles check within $\pm 100^{\circ}$ R for all runs. The wall temperature profile as measured with the tungsten - tungsten-26-percent-rhenium thermocouple is then verified.

Average Friction Factors

Static-pressure taps are located only at the entrance and near the exit of the test section. Consequently, only average friction factors can be calculated. The location of the exit pressure tap in the plates precludes an exit pressure loss. The pressure drop measured across the test section is made up of four components: entrance, momentum, friction, and spacer pressure drop. The pressure drops at the test-section entrance and the spacer entrance are made up of two components: a pressure loss due to a change in flow area and a

loss due to the irreversible free expansion, as characterized by the vena contracta following an abrupt contraction. The spacer exit pressure drop is also made up of two components: a pressure rise due to a change in flow area and a pressure loss associated with the irreversible free expansion and momentum changes following an abrupt expansion. These relations are best expressed by equations (1) to (5), which are modifications of those given in reference 9:

$$\Delta P = \frac{G^2}{2g}\left[\left(K_c + 1 - \sigma^2\right)\frac{1}{\rho_0} + 2\left(\frac{1}{\rho_5} - \frac{1}{\rho_0}\right) + f_b\,\frac{S_{fr}}{A_{fr}}\,\frac{1}{\rho_m} + Z\right] \qquad (1)$$

(Entrance) (Momentum) (Friction) (Spacer)

where Z is the pressure factor from the spacer entrance and the exit, defined for the two sets of spacers illustrated in figure 3 as

$$Z = \left(K_{cs,1} + 1 - \sigma^2\right)\frac{1}{\rho_1} + \left(K_{cs,3} + 1 - \sigma^2\right)\frac{1}{\rho_3} - \left[\left(-K_{es,2} + 1 - \sigma^2\right)\frac{1}{\rho_2} + \left(-K_{es,4} + 1 - \sigma^2\right)\frac{1}{\rho_4}\right] \qquad (2)$$

Since the density change across any set of spacers is small, equation (2) may be simplified by setting $\rho_1 = \rho_2$ and $\rho_3 = \rho_4$:

$$Z = \left(K_{cs,1\text{-}2} + K_{es,1\text{-}2}\right)\frac{1}{\rho_{1\text{-}2}} + \left(K_{cs,3\text{-}4} + K_{es,3\text{-}4}\right)\frac{1}{\rho_{3\text{-}4}} \qquad (3)$$

Typical values of K_{cs} and K_{es}, the spacer contraction and expansion coefficients, respectively, are given for a similar configuration as a function of Reynolds number and the ratio of the free flow area to the frontal area σ in reference 9. The change in the values of K_{cs} and K_{es} for the range of Reynolds numbers encountered in this report is small. Therefore, if a mean density is used, equation (3) can be further simplified to

$$Z = N\left(K_{cs} + K_{es}\right)\frac{1}{\rho_m} \qquad (4)$$

where N is the number of sets of spacers. A value of 0.15 was used for the sum of the term $(K_{cs} + K_{es})$. When equation (4) is substituted into equation (1), a generalized form of the equation is obtained to determine the average friction factor:

$$\Delta P = \frac{G^2}{2g}\left[\left(K_c + 1 - \sigma^2\right)\frac{1}{\rho_0} + 2\left(\frac{1}{\rho_{n+1}} - \frac{1}{\rho_0}\right) + f_b\,\frac{S_{fr}}{A_{fr}}\,\frac{1}{\rho_m} + N\left(K_{cs} + K_{es}\right)\frac{1}{\rho_m}\right] \qquad (5)$$

(Entrance) (Momentum) (Friction) (Spacer)

The mean density for equation (5) is evaluated from the static pressures and temperatures of the gas as follows:

$$\rho_m = \frac{1}{\mathcal{R}_g}\left(\frac{p_0 + p_{n+1}}{t_0 + t_{n+1}}\right) \tag{6}$$

The absolute static temperatures t_0 and t_{n+1} used in evaluating the mean density are calculated from measured gas flow, static pressure, and total temperature by the following equation:

$$t = -\frac{\gamma g}{(\gamma - 1)\mathcal{R}_g}\left(\frac{p}{G}\right)^2 + \sqrt{\left[\frac{\gamma g}{(\gamma - 1)\mathcal{R}_g}\left(\frac{p}{G}\right)^2\right]^2 + 2T\,\frac{\gamma g}{(\gamma - 1)\mathcal{R}_g}\left(\frac{p}{G}\right)^2} \tag{7}$$

which is obtained by combining the perfect gas law, the equation of continuity, and the energy equation for an inviscid fluid.

The friction factor is then evaluated at film temperature T_f by the relation

$$f_f = \frac{2g\,\Delta P_{fr}}{\dfrac{S_{fr}\rho_f G^2}{A_{fr}\rho_m^2}} = \frac{\rho_m}{\rho_f} f_b = \frac{2T_f}{t_{in} + t_{out}} f_b \tag{8}$$

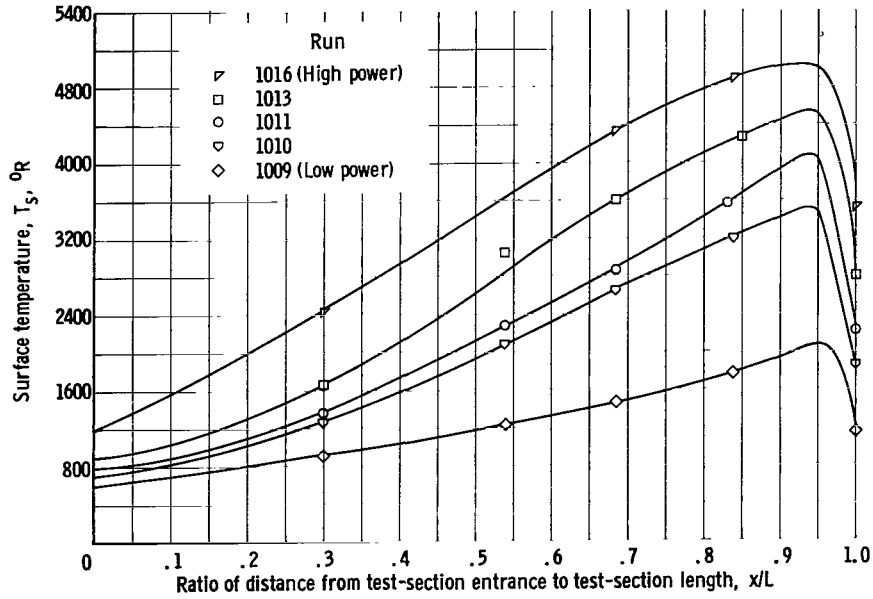

Figure 8. - Surface temperature profiles for various amounts of heat input for laminar-flow runs. Hydrogen mass-flow rate, 0.0082 pound per second.

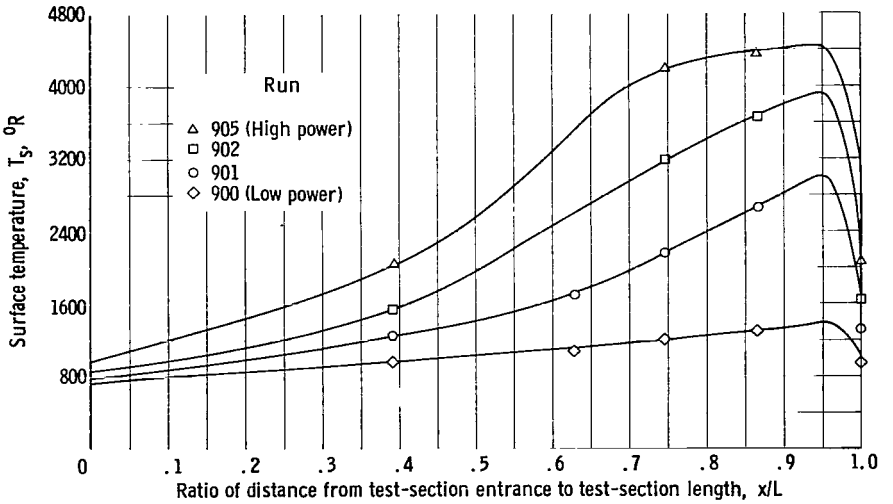

Figure 9. - Surface temperature profiles for various amounts of heat input for turbulent-flow runs. Hydrogen mass-flow rate, 0.023 pound per second.

Run	Inlet gas temperature, °R	Outlet gas temperature, °R	Inlet gas pressure, lb/sq in. abs	Pressure drop across test section, lb/sq in.	Voltage across test section, v	Current through test section, amp	Gas flow, lb/sec	Film Reynolds number, Re_f	
								At entrance	At exit
900	541	955	30.0	9.00	3.38	10,800	0.0231	12,752	8767
901	541	1336	34.8	11.93	6.20	11,800		12,924	4070
902	541	1625	37.1	12.80	8.60	12,000		9,846	3383
903	540	1844	38.6	13.60	10.25	12,160		------	----
904	541	1955	39.7	14.30	11.10	12,240		------	----
905	542	2044	41.2	15.02	11.70	12,400		8,371	3766
906	542	2105	42.7	16.60	12.40	12,500		-----	----
907	541	2215	44.6	18.15	13.40	12,800		-----	----
908	540	2435	46.4	18.85	14.40	12,880		-----	----
1009	526	1165	18.1	2.10	2.88	7,520	.0081	5,169	2156
1010	526	1845	20.1	3.50	5.30	8,720	.0081	4,458	1486
1011	528	2190	21.1	4.15	6.38	9,000	.0081	3,956	1354
1012	526	2530	22.0	4.80	7.58	9,200	.0082	-----	----
1013	528	2790	22.7	5.30	8.50	9,400	.0081	3,517	1295
1014	527	3008	23.2	5.70	9.25	9,520	.0082	-----	----
1015	526	3241	23.9	6.35	10.50	9,760	.0082	-----	----
1016	526	3480	24.7	6.80	11.50	9,880	.0082	2,437	1257
[a]1101	528	1029	21.4	3.95	3.08	9,080	.0125	-----	----
1102	528	1383	23.1	4.90	4.55	9,800		-----	----
1103	528	1648	24.4	5.70	5.97	10,080		-----	----
1104	528	2001	25.8	6.80	7.55	10,360		-----	----
1105	528	2193	26.8	7.50	8.55	10,520		-----	----
1106	528	2404	27.8	8.30	9.60	10,720		-----	----
1107	525	2620	29.0	9.25	10.60	10,800		-----	----
1108	525	2860	29.9	9.90	11.50	11,040		-----	----

[a]Wall temperature profiles were not measured for the 1100 series runs.

RESULTS AND DISCUSSION

Data are presented for three flow rates. Associated with two of the flow rates are the representative axial wall temperature profiles for all five plates shown in figures 8 and 9. The significant dimensions of the test section were as follows:

Equivalent diameter at spacer cross section, D, ft	0.00935
Equivalent diameter at spacerless cross section, D_{fr}, ft	0.010
Length-diameter ratio, L/D	74
Heat-transfer surface area, S, sq ft	0.745
Friction surface area, S_{fr}, sq ft	0.835

The measured parameters are listed in the preceding table. The following are the restrictions and the assumptions under which the data were obtained:

(1) The temperature-dependent hydrogen properties are evaluated at the film temperature. As a result, the modified Reynolds number decreases as much as a factor of 3 from entrance to exit of the test section for a given flow rate.

(2) Uneven flow blockage exists through the passages. The four inner passages contain 0.060- by 0.120-inch spacers to support the plates against the electromagnetic forces, whereas the outer passages contain only heads and nuts of the spacer pins.

(3) The test section and boron nitride housing provide four inner flow passages, each having two heated surfaces, and two outer flow passages, each having one heated surface and one surface that acts as an adiabatic wall. This causes the thermal boundary layer to build up on only one heated surface in an outer passage, which results in a gas temperature profile different from that for an inner passage. Reference 10 compares the Nusselt number for heating on one wall and on both walls. Also, the hydrogen flow rate per passage adjusts itself such that the pressure drop per passage is equal. An outer passage, because of the higher gas density and lower velocity, has a calculated mass flow as much as 50 percent greater than an inner passage.

(4) The heat-transfer surface area and the test-section length are not the same as the frictional surface area and the frictional length. Therefore, two evaluations of equivalent diameter are necessary. The diameters are defined as

$$D = \frac{4A}{S/L} \tag{9a}$$

$$D_{fr} = \frac{4A_{fr}}{S_{fr}/L_{fr}} \tag{9b}$$

Also, the friction equation (1) contains an entrance- and an exit-pressure-drop term across each set of spacers. Therefore, the mass velocity for frictional calculations is based on the spacerless cross-sectional flow area. The heat-transfer mass velocity is calculated at the minimum-free-flow area or spacer

cross section as outlined in reference 9. These considerations are included in the heat-transfer and friction calculations.

(5) Steady-state conditions are assumed, and free-convection and radiation effects are neglected. A calculation outlined in reference 3 indicates that the free-convection effects are negligible.

(6) The fact that the heated portion of the test-section length is 74 L/D precludes fully developed velocity profiles over a considerable length for the Reynolds numbers of these tests.

(7) The hydrodynamic boundary layer starts before the thermal boundary layer. The velocity profile starts to build up 6 L/D before the heated test section. Consequently, the thermal and velocity boundary layers do not develop simultaneously.

Heat-Transfer Correlation in Laminar-Flow Entrance Region

There is growing interest in compact heat exchangers employing large ratios of surface to volume (equivalent diam., approx. 1/8 in.) with low-density gas. The literature lists several solutions for constant-property local Nusselt numbers in the entrance region of heated tubes and plates for heat-generation conditions such as constant wall temperature and constant heat flux

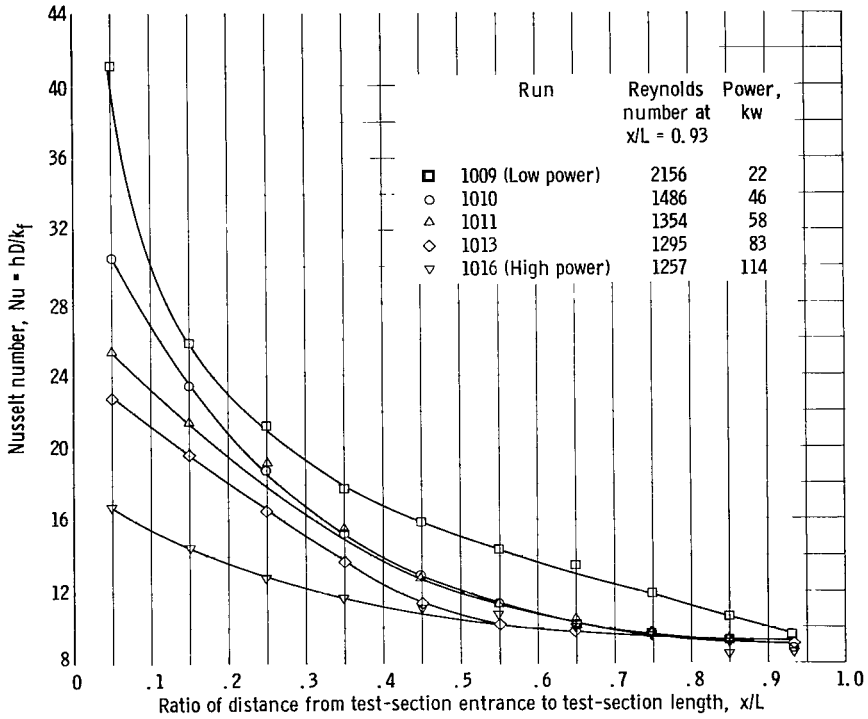

Figure 10. - Variation of local laminar Nusselt number along test-section length for various heat inputs. Hydrogen mass-flow rate, 0.0082 pound per second.

(refs. 10 to 14). Exact mathematical analysis, however, is difficult, with variable properties or under the restrictions listed at the beginning of this discussion.

The laminar heat-transfer data reported herein are for the entrance region of flat parallel plates, where both the velocity profile and the thermal boundary layers are developing. The flow rate for the laminar-flow runs was 0.0082 pound per second of hydrogen. Five axial temperature profiles measured with thermocouples are shown in figure 8. Figure 10 is a plot of local Nusselt number against x/L. The conventional plot of Nusselt number against the reciprocal of Graetz number is shown in figure 11. Low- and high-power runs refer to

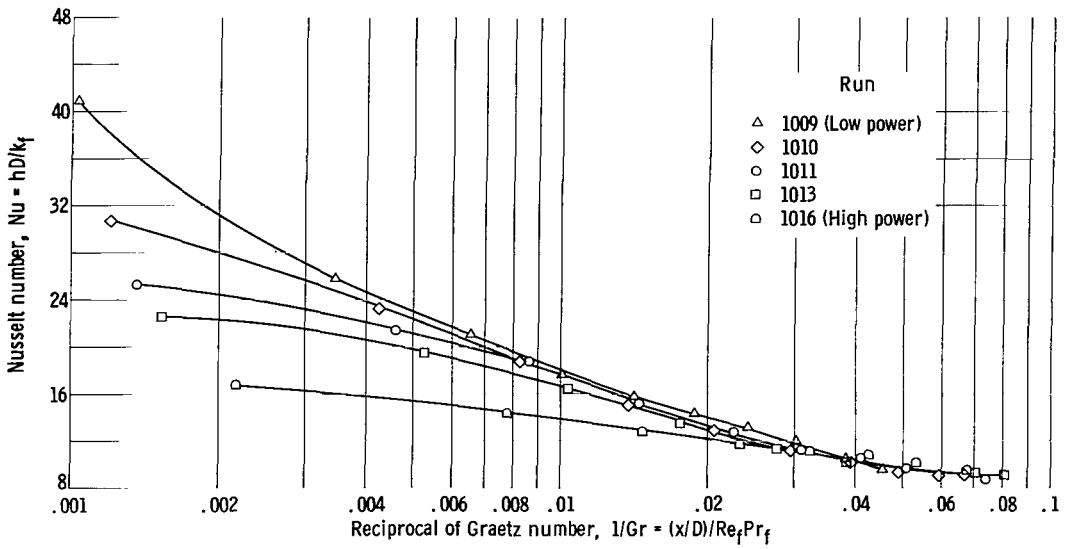

Figure 11. - Variation of Nusselt number with reciprocal of Graetz number. Hydrogen mass-flow rate, 0.0082 pound per second.

the corresponding profiles for low and high wall temperature of figure 8. As the power to the test section is progressively increased (and wall temperature rises), the value of the local Nusselt number (fig. 10) decreases for a given x/L in the entrance region, where the velocity and thermal boundary profiles are developing. These trends can be explained by referring to figure 12, which presents curves based on the analysis of reference 11 (data from ref. 12). Figure 12 shows the relative local Nusselt numbers for circular tubes for both a fully developed parabolic velocity profile and a developing velocity profile based on Langhaar's velocity profiles (ref. 11). Both curves are for a Prandtl number of 0.7 and constant wall temperature and fluid properties.

The relative positions of the two curves of figure 12 are considered. The Langhaar developing velocity profile curve is higher than the fully developed parabolic velocity curve. It follows that the low-power curve in figure 11 can be compared with the Langhaar developing velocity profile curve in the region of transition from slug to parabolic flow because the change in fluid properties due to moderate temperature near the wall is not very severe. In the high-power curve, however, the high wall temperatures heat the hydrogen near the wall and thus increase its viscosity. This results in a parabolic velocity

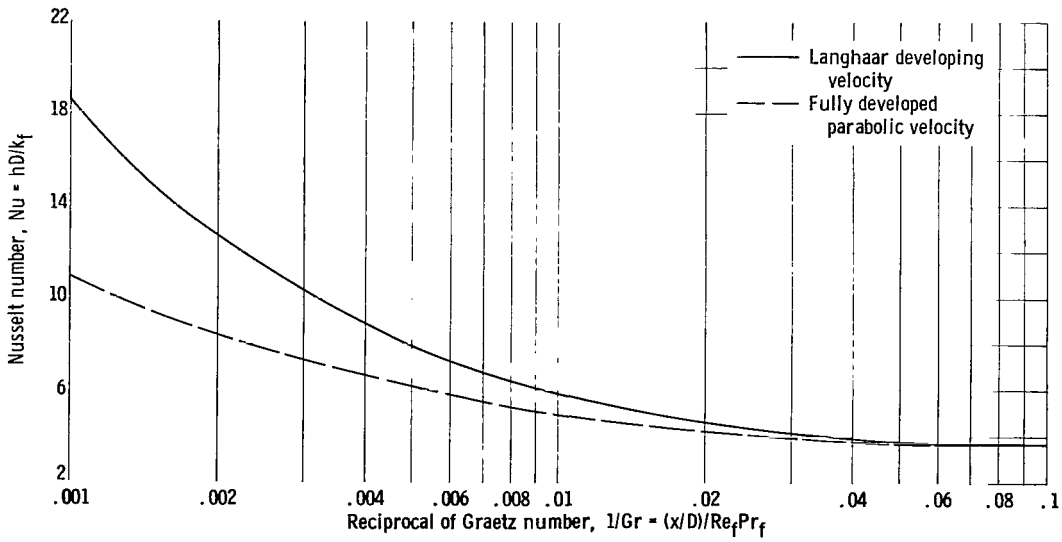

Figure 12. - Kay's numerical solutions of local Nusselt number plotted against reciprocal of Graetz number for constant wall temperature (data from ref. 12). Circular tubes; Prandtl number, 0.7; constant properties.

profile in the fluid layers near the wall, but not throughout the core. Consequently, the high-power curve in the region of the wall can be compared with the fully developed parabolic velocity profile. The relative trend of the curves of figures 10 and 11 can be partially explained by the change in velocity profile. Flow in the entrance region of parallel plates, however, can be compared with flow over a flat plate (ref. 15) wherein Nu_x is proportional to $\sqrt[3]{Pr}\sqrt{Re_x}$. Even though the flow rate is constant, because of property variation, the local Reynolds number is much higher for the low-power curve than for the high-power curve. Thus, a thinner thermal boundary layer or a higher Nusselt number is produced.

The following table (from ref. 16) lists the constant property values of Nusselt number for fully developed laminar flow under varied conditions of geometry, velocity distribution, and wall temperature distribution. Certain trends can be seen from the table by keeping two of the parameters constant and varying the third. For example, when geometry is varied, it can be seen that a parallel-plate configuration produces a higher Nusselt number than a tube configuration for the same velocity distribution and wall conditions. For a given geometry and

Geometry	Velocity distribution	Wall condition	Nusselt number, hD/k
Circular tube	Parabolic	Heat flux constant	4.36
Circular tube	Parabolic	Surface temperature constant	3.66
Circular tube	Slug (uniform)	Heat flux constant	8.00
Circular tube	Slug (uniform)	Surface temperature constant	5.75
Parallel plates	Parabolic	Heat flux constant	8.23
Parallel plates	Parabolic	Surface temperature constant	7.60
Parallel plates[a]	Varying	Heat flux and surface temperature both increase in axial direction	9.0

[a]Experimental results of present investigation.

given wall conditions, slug or uniform flow produces a higher Nusselt number than does parabolic flow. Wall conditions also affect the local Nusselt numbers. In figure 13 is seen a comparison of Kay's numerical values of local

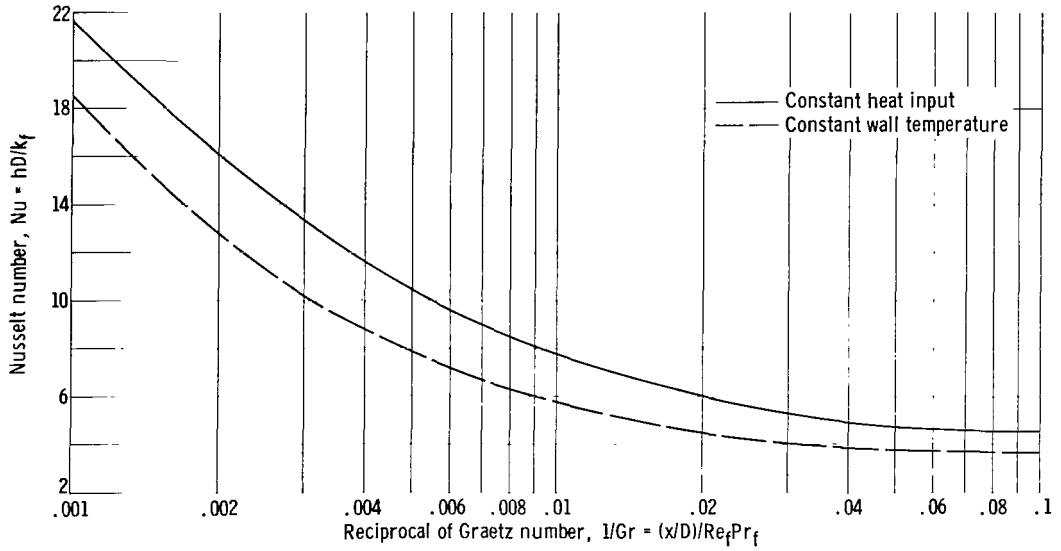

Figure 13. - Kay's numerical solution of local Nusselt number plotted against reciprocal of Graetz number for varying modes of wall temperature distribution (data from ref. 12). Prandtl number, 0.7; constant properties; Langhaar developing velocity.

Nusselt numbers in a tube for wall conditions of constant heat input with those for constant wall temperature. Variation of surface temperature along the x-axis influences the shape of the temperature profile and also the boundary-layer thickness. The effect of geometry, velocity distribution, and wall conditions are summarized in the table on page 19.

For this investigation an experimental value of 9.0 was determined as the constant Nusselt number for fully developed laminar flow (note the asymptote of fig. 11). This is in agreement with the analytical values listed in the table on page 19 when the interdependency of geometry, wall conditions, and velocity distribution are considered.

For two-dimensional steady flow between parallel plates where there is nonisothermal heat addition in the entrance region, the temperature of the fluid changes from a uniform low value to varying values along the flow path. In addition to the velocity boundary layer, which in this particular investigation began 6 L/D before the heated section, a thermal boundary layer develops in the entrance region (generally $\Delta_t \approx \delta$). The relative rate of development depends on the Prandtl number of the fluid. The thermal entrance length is the distance from the beginning of the region of heat addition to the point where the Nusselt number becomes independent of length.

The data of the present investigation indicate that the thermal entrance length depends on the local modified Reynolds number with properties evaluated at the film temperature. In figure 10 it is noted that four of the five curves of the local Nusselt number as a function of x/L approach a constant Nusselt number at a shorter x/L as the local modified Reynolds number decreases. If

this x/L position is converted into an L/D term and put into the form $L/D = CRe_f$, the value of C for this investigation varies from 0.035 to 0.040. This can also be seen in figure 11 where it can be seen that four of the five experimental curves level out at a constant reciprocal of Graetz number, or as expressed in equation form, $(x/D)/Re_f Pr_f$ = constant. For a constant Prandtl number x/D is proportional to the modified local film Reynolds number. The low-power curves of figures 10 and 11 do not reach a constant Nusselt number or a constant reciprocal of Graetz number because the test section is too short. For example, if the exit Reynolds number of 2156 for this low-powered run remained a constant, it would take approximately 80 L/D for the Nusselt number to become constant in figure 10. It is also interesting to note that various investigators listed in reference 17 expressed the L/D for a velocity profile to become fully developed in laminar flow with constants ranging from $C = 0.0287$ to 0.0575.

Friction Factor

The friction factor is defined as the equivalent shear force per unit area in the flow direction. A treatment of the friction factor in the entrance region of short ducts in laminar flow is particularly complicated. For example, friction factor

$$f = \frac{\tau_w}{\frac{\rho V^2}{2g}}$$

is defined on the basis of wall shear stress and is for fully developed flow.

The detailed calculations of the average friction factor, including spacer correction, has been covered in the section METHOD OF CALCULATION. An additional discussion is needed, however, in order to explain the trend of the data.

The following equation, taken from reference 16, is used to calculate the friction factor:

$$p_2 - p_1 = \frac{G^2}{2g\alpha}\left(\frac{1}{\rho_2} - \frac{1}{\rho_1}\right) + \frac{2f}{g}\frac{L}{D}\frac{G^2}{\rho_m} \qquad (10)$$

(Static pressure across test section) (ΔP_{mo}) (ΔP_{fr})

It is noted that ρ_m, as defined in equation (6), was used because it produced a satisfactory correlation. The mode of heat generation will determine which method of density calculation will give the best approximation to an integrated density, whether it be arithmetic, reciprocal $\left(\frac{1}{\rho} = \frac{1}{2}\left(\frac{1}{\rho_1} + \frac{1}{\rho_2}\right)\right)$, or one defined

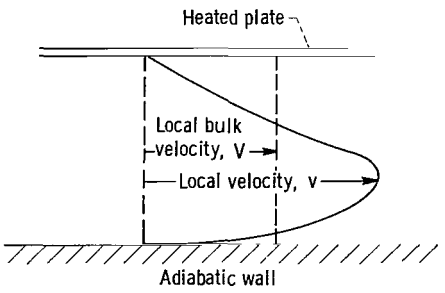

Figure 14. - Asymmetric velocity profile.

by equation (6). To determine the average friction factor as defined in equation (10), both α and the integrated value of ρ must be known. Alpha is a correction to be applied when the velocity profile deviates from a uniform shape.

If the velocity varies in the manner shown in figure 14, the momentum is not equal to ρAV^2 but is represented as $\rho AV^2/\alpha$, where

$$\alpha = \frac{\rho AV^2}{\int_A v(\rho v \, dA)} \tag{11}$$

When the velocity is uniform, $\alpha = 1$. For the laminar-flow runs of this investigation, the velocity profile is developing for at least half of the test-section length, as evidenced by the curves of figure 10 (p. 17). A variable α should be used because the velocity profile is continuously changing as a result of both entrance effects and property variation.

Reference 9 gives curves of a momentum correction factor that can be used to convert the actual momentum rate to that which would be obtained from the mean velocity. These data are for circular tubes with constant properties. This factor of reference 9, which is the reciprocal of α, reaches a maximum of 1.33.

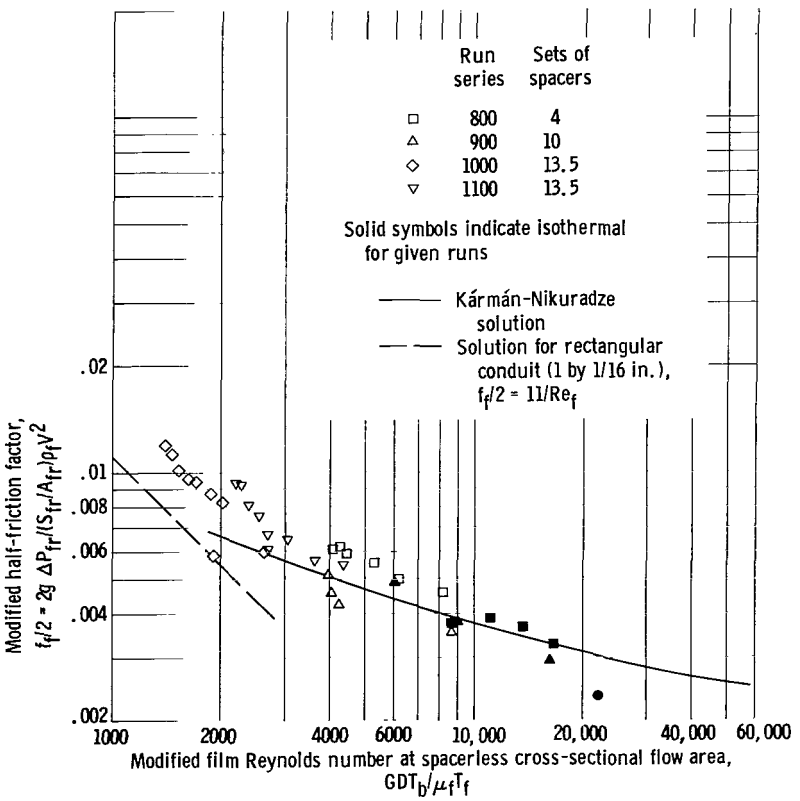

Figure 15. - Correlation of average modified half-friction factors with modified Reynolds number. Viscosity and density of hydrogen evaluated at film temperature; spacer contraction plus spacer expansion coefficient, 0.15.

Most experimental investigators assume α to be a constant equal to 1. For highly turbulent flow, this is a good approximation. In figure 15, the 1100 series runs illustrate that, when α is assumed equal to 1 as in the present investigation, the modified friction data for variable fluid properties tend to be progressively higher as the heat generation is increased for a given flow rate. Because the velocity profiles are not known throughout the test section, a value of α is not calculated but is assumed to be equal to 1.

This same trend can be seen in the data of references 1 to 3. This is particularly evident at Reynolds numbers below 5000, where α is less than 1. Consequently, the ΔP_{mo} calculated from equation (10), which varies from 25 to 50 percent of the total measured ΔP, is too low and results in too high a value of friction factor. Because the velocity profile is more pointed with increased heat generation, for a given flow rate, a smaller value of α should be used.

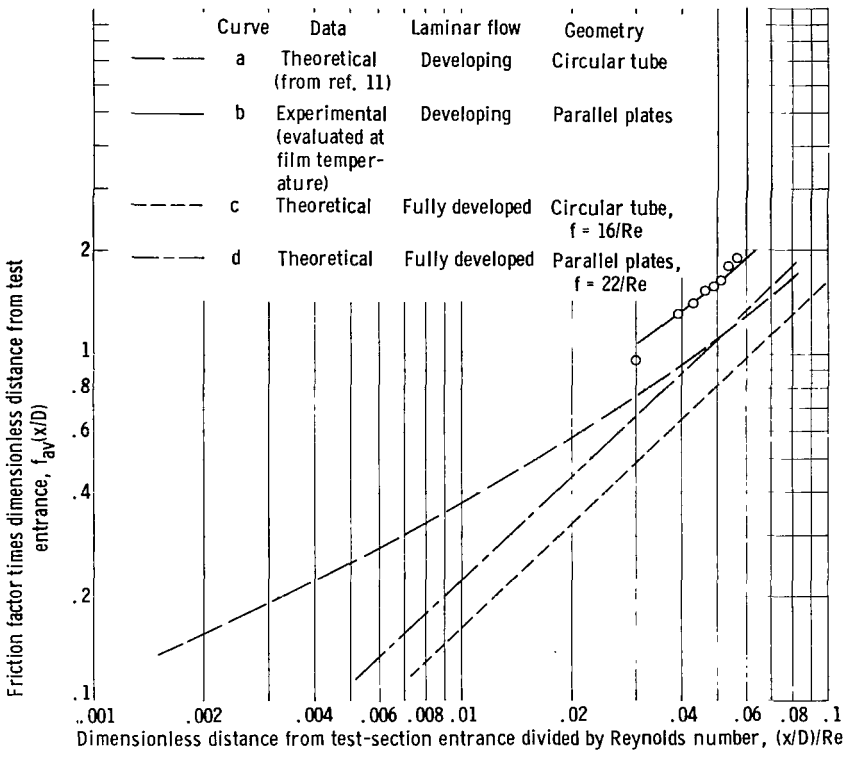

Figure 16. - Average laminar-flow friction factors in entrance region for developing and fully developed laminar flow for circular tube and parallel plates.

Laminar flow. - In figure 16, the following friction factors are plotted against Reynolds number: (a) Langhaar's theoretical friction factors for laminar flow in the entrance region of a circular tube (ref. 11), (b) experimental laminar friction factors of this investigation, (c) friction factors for fully developed laminar flow in a circular tube, and (d) friction factors for fully developed laminar flow for a rectangular duct of the geometry used in this investigation.

If the ratios of the curves a/c and b/d are compared, it is found that these ratios are approximately the same. Although the entrance region does not extend the entire length of the channel, these ratios establish that the pressure drop in the entrance region is appreciable. As a result, the average values of friction factor calculated over the test-section length should be larger than those for fully developed laminar flow.

Turbulent flow. - In figure 15 is plotted $(f/2)_f$ against modified film Reynolds number. As previously noted, most of the data fall above the predicted Kármán-Nikuradse line. On the other hand, the isothermal data correlate well since the velocity profile at the wall is not affected by the viscous forces associated with heating, and the Reynolds number is higher for the same flow rates. In general, most investigators have found good agreement with the predicted line at higher bulk Reynolds numbers (above 10,000) but only fair agreement in the bulk Reynolds number range 2000 to 10,000. Although it is true that $\alpha \approx 1$ for fully developed turbulent flow and constant properties, it is possible that variable properties alter the shape of the velocity profile

sufficiently to change the value of α, and thus give too low a momentum pressure drop and too high a value of friction factor, especially in this low Reynolds number region.

Heat Transfer in Turbulent Flow

The turbulent heat-transfer data are developed from four variable-power runs at a hydrogen flow rate of 0.023 pound per second. Since Reynolds numbers based on bulk gas temperatures vary from 9000 to 14,000 (3000 to 12,500 on a modified film basis), flow in these runs is characterized as turbulent. Local heat-transfer coefficients are calculated because of the extreme variation in properties throughout the test section.

Figures 17 and 18 (based on run 905) illustrate the typical axial trends

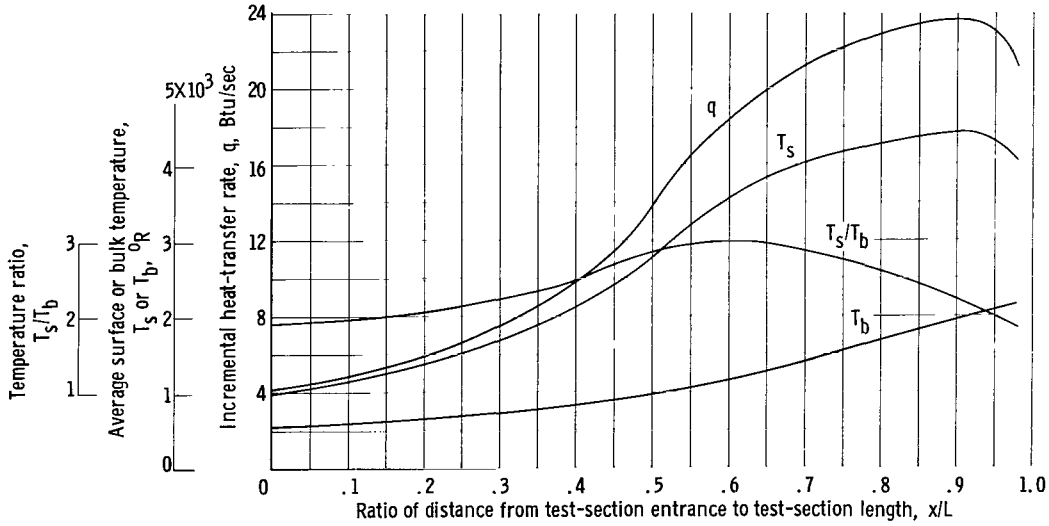

Figure 17. - Typical variation of temperatures and heat rate with test-section length for turbulent flow. Hydrogen mass-flow rate, 0.023 pound per second.

of the more significant variables along the test-section length. The heat flux q increases through about 95 percent of the length of the test section and then drops off over the last 5 percent because of conduction losses through the electrical bus connections. The interdependence of heat generation q, surface temperature T_s, and bulk gas temperature T_b for a given gas flow rate is shown. Because the gas temperature increases throughout the length of the test section, the Reynolds number, reflecting the effect of viscosity, decreases through about 90 percent of the test-section length and then levels off. The Nusselt number decreases with the Reynolds number through about 80 percent of the test-section length and then levels off or increases slightly as the effect of Prandtl number and the ratio of surface to bulk gas temperature T_s/T_b becomes more significant. The heat-transfer coefficient h first decreases and then increases throughout the test-section length and thereby reflects inversely the effect of T_s/T_b as reported in reference 1.

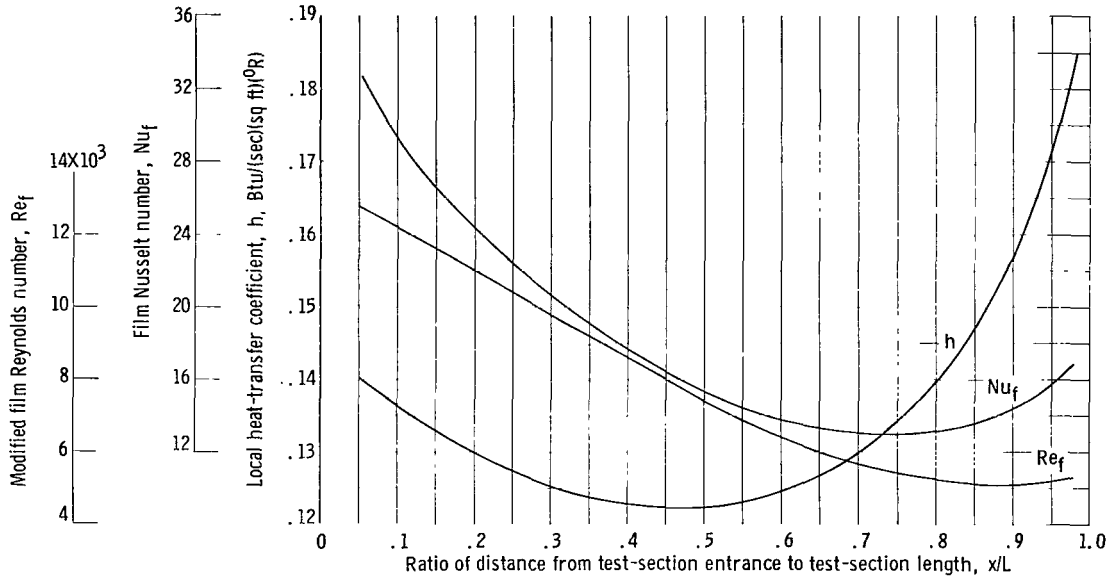

Figure 18. - Typical variation of Reynolds number, Nusselt number, and heat-transfer coefficient with test-section length for turbulent flow. Hydrogen mass-flow rate, 0.023 pound per second.

The local heat-transfer coefficients are calculated on the basis of the measured surface temperature profile shown in figure 9 (p. 15). The data may be characterized by the power inputs to the gas. Run 900 represents the lowest power run and approximates constant-property conditions. Runs 901, 902, and 905 represent progressively higher power inputs and hence greater deviations from constant-property conditions. The data are best correlated by the following Dittus-Boelter equation:

$$\frac{hD}{k_f} = 0.023\left(\frac{G_{max}D}{\mu_f}\right)^{0.8}\left(\frac{T_b}{T_f}\right)^{0.8}\left(\frac{c_{p,f}\mu_f}{k_f}\right)^{0.4} \tag{12}$$

with the fluid properties evaluated at the film temperature (fig. 19). All of these data correlate within +16 percent and -6 percent of the previous equation, the majority (70 percent) of the data correlating within ±6 percent. The data that deviate most are in the region of 20 diameters or less from the entrance which indicates an entrance effect.

The data from the low-power run (900) do not correlate as well as the data from the higher power runs. One reason suggested for this discrepancy is that the number of spacers used in the test section may cause greater turbulence at the higher Reynolds numbers and increase the heat transfer.

The fact that the majority of the data do correlate with the standard equation even with the added turbulence caused by the spacers is significant and indicates that the effect of spacers can be accounted for by basing the mass velocity on the minimum cross-sectional flow area and by assuming the

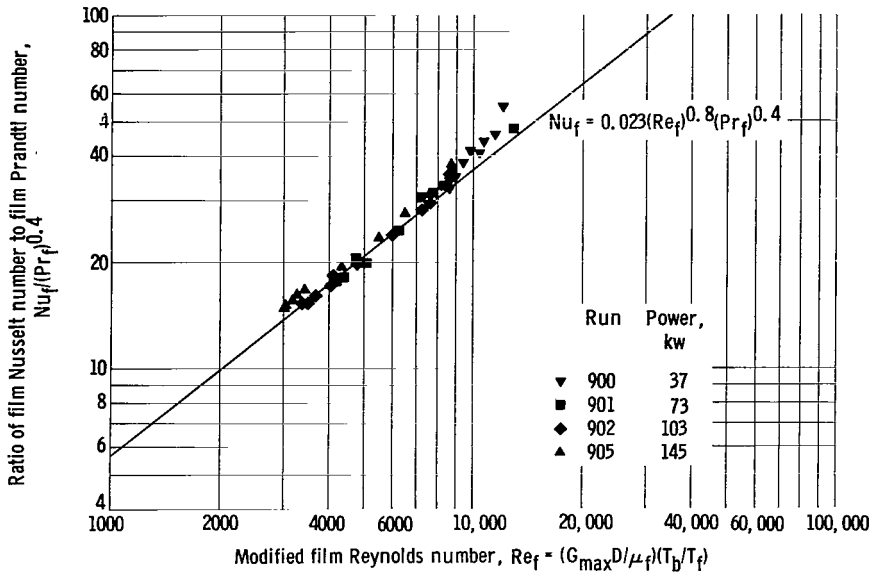

Figure 19. - Correlation of local turbulent heat-transfer coefficients. Hydrogen mass-flow rate, 0.023 pound per second.

spacer to be part of the heat-transfer surface area.

SUMMARY OF RESULTS

The following results were obtained in investigation of local heat-transfer coefficients and average friction factors for turbulent and laminar flow of hydrogen over parallel tungsten plates at surface temperatures up to 5000° R:

1. Local laminar Nusselt numbers in the entrance region of parallel plates exhibited a decided decrease with an increase in heat generation.

2. The thermal entrance length required for the local laminar Nusselt number to approach a constant, at a constant flow rate, was a function of the local modified film Reynolds number, which decreased as much as a factor of 3 from the entrance to the exit of the test section.

3. The value of Nusselt number for fully developed laminar flow across parallel plates was determined experimentally to be 9. This number is in reasonable agreement with analytical results.

4. Local turbulent heat-transfer coefficients in a parallel-plate configuration with surface temperatures as high as 5000° R and ratios of surface to bulk temperature as high as 3.0 correlated well with those calculated by using a Dittus-Boelter type equation with properties evaluated at the film temperature. The effect of spacers and other support members in the heat-transfer section can be accounted for by basing the mass velocity on the minimum cross-

sectional flow area and by assuming the spacers to be part of the heat-transfer surface area.

5. Average turbulent isothermal friction factors correlated well with the Kármán-Nikuradse curve. With the addition of heat, however, the modified friction factors for a given flow rate became progressively higher because of changes in the velocity profile resulting from variations in hydrogen properties.

6. A comparison of laminar friction factors of this investigation in the developing region with fully developed friction factors in parallel plates showed the same trend as the analytical results of Langhaar for developing and fully developed constant-property friction factors in a tube.

Lewis Research Center
National Aeronautics and Space Administration
Cleveland, Ohio, April 20, 1964

REFERENCES

1. Humble, Leroy V., Lowdermilk, Warren H., and Desmon, Leland G.: Measurements of Average Heat-Transfer and Friction Coefficients for Subsonic Flow of Air in Smooth Tubes at High Surface and Fluid Temperatures. NACA Report 1020, 1951.

2. Taylor, Maynard F.: Local Heat-Transfer Measurements for Forced Convection of Hydrogen and Helium at Surface Temperatures up to 5600° R. NASA, Lewis Research Center. Presented at Heat Transfer and Fluid Mechanics Institute, Pasadena (Calif.), June 13-14, 1963.

3. Davenport, Monty E.: The Effect of Transverse Temperature Gradients on the Heat Transfer and Friction for Laminar Flow of Gases. TR 247-3, Stanford Univ. (TID-17792), 1962.

4. McEligot, Donald M.: Effect of Large Temperature Gradients on Turbulent Flow of Gases in the Downstream Region of Tubes. TR 247-5, Stanford Univ. (TID-19446), 1963.

5. Dwight, Herbert B.: Electrical Coils and Conductors, Their Electrical Characteristics and Theory. McGraw-Hill Book Co., Inc., 1945.

6. Den Hartog, J. P.: Mechanical Vibrations. Third Ed., McGraw-Hill Book Co., Inc., 1947.

7. Anon.: Thermocouples and Thermocouple Extension Wires. Instrument Society of America, Revised composite of RP 1.9 - RP 1.7, July, 1959.

8. Grier, Norman T.: Calculation of Transport Properties and Heat-Transfer Parameters of Dissociating Hydrogen. NASA TN D-1406, 1962.

9. Kays, W. M., and London, A. L.: Compact Heat Exchangers. The National Press, 1955.

10. Sparrow, E. M.: Analysis of Laminar Forced-Convection Heat Transfer in Entrance Region of Flat Rectangular Ducts. NACA TN 3331, 1955.

11. Langhaar, Henry L.: Steady Flow in the Transition Length of a Straight Tube. J. Appl. Mech., vol. 9, 1942, pp. A-55-A-58.

12. Kays, W. M.: Numerical Solutions for Laminar-Flow Heat Transfer in Circular Tubes. Trans. ASME, vol. 77, 1955, pp. 1265-1274.

13. Sellars, J. R., Tribus, Myron, and Klein, J. S.: Heat Transfer to Laminar Flow in a Round Tube or Flat Conduit - The Graetz Problem Extended. Trans. ASME, vol. 78, 1956, pp. 441-448.

14. Norris, R. H., and Streid, D. D.: Laminar-Flow Heat-Transfer Coefficients for Ducts. Trans. ASME, vol. 62, 1940, pp. 525-533.

15. Eckert, Ernst R. G., and Drake, Robert M., Jr.: Heat and Mass Transfer, McGraw-Hill Book Co., Inc., 1959.

16. Rohsenow, Warren M., and Choi, Harry Y.: Heat, Mass, and Momentum Transfer. Prentice Hall, 1961.

17. Knudsen, James G., and Katz, Donald L.: Fluid Dynamics and Heat Transfer. McGraw-Hill Book Co., Inc., 1958.

NASA-Langley, 1964 E-2314

2/17/85

"The aeronautical and space activities of the United States shall be conducted so as to contribute . . . to the expansion of human knowledge of phenomena in the atmosphere and space. The Administration shall provide for the widest practicable and appropriate dissemination of information concerning its activities and the results thereof."

—NATIONAL AERONAUTICS AND SPACE ACT OF 1958

NASA SCIENTIFIC AND TECHNICAL PUBLICATIONS

TECHNICAL REPORTS: Scientific and technical information considered important, complete, and a lasting contribution to existing knowledge.

TECHNICAL NOTES: Information less broad in scope but nevertheless of importance as a contribution to existing knowledge.

TECHNICAL MEMORANDUMS: Information receiving limited distribution because of preliminary data, security classification, or other reasons.

CONTRACTOR REPORTS: Technical information generated in connection with a NASA contract or grant and released under NASA auspices.

TECHNICAL TRANSLATIONS: Information published in a foreign language considered to merit NASA distribution in English.

TECHNICAL REPRINTS: Information derived from NASA activities and initially published in the form of journal articles.

SPECIAL PUBLICATIONS: Information derived from or of value to NASA activities but not necessarily reporting the results of individual NASA-programmed scientific efforts. Publications include conference proceedings, monographs, data compilations, handbooks, sourcebooks, and special bibliographies.

Details on the availability of these publications may be obtained from:

SCIENTIFIC AND TECHNICAL INFORMATION DIVISION

NATIONAL AERONAUTICS AND SPACE ADMINISTRATION

Washington, D.C. 20546